Astron. Astrophys. 363, 933–946 (2000)

ASTRONOMY AND ASTROPHYSICS

IRAS galaxies in the Perseus cluster

H. Meusinger[⋆]**, J. Brunzendorf, and R. Krieg**

Thüringer Landessternwarte Tautenburg, 07778 Tautenburg, Germany

Received 21 August 2000 / Accepted 28 September 2000

Abstract. We cross-correlate the optical catalogue of galaxies in the field of the Perseus cluster (Abell 426) with IRAS PSC sources. The optical catalogue comprises data on 660 galaxies brighter than $B_{25} \approx 19.5$ (Brunzendorf & Meusinger 1999). A sample of 19 IRAS galaxies is found. According to their redshifts, 17 galaxies are likely members of the Perseus cluster, two are background galaxies. The sample-averaged FIR excess is higher than expected for normal galaxies. The optical morphology of the IRAS galaxies is evaluated on CCD images taken in the B band at a seeing of about $1''$, complemented by CCD images taken in the redshifted Hα band or in the R band. Individual descriptions are presented along with the B band images for all of the IRAS galaxies. A substantial fraction of the galaxies in the IRAS sample exhibit signs for morphological distortion. A correlation between the FIR activity and the strength of distortion is indicated. On the other hand, there are approximately as many disturbed/interacting galaxies in the Perseus cluster region without IRAS counterparts as IRAS galaxies. The IRAS galaxies are much less concentrated towards the cluster centre than typical bright cluster galaxies. For the distorted non-IRAS galaxies, such a trend is less pronounced. These differences may be related to rapid stripping of gas as galaxies enter the cluster.

Key words: galaxies: clusters: individual: Perseus – galaxies: interactions – galaxies: peculiar – galaxies: starburst – infrared: galaxies

1. Introduction

The Perseus cluster (A 426) is a nearby rich galaxy cluster of Bautz-Morgan class II-III and Rood-Sastry type L. Due to its proximity and richness, it is suited for the investigation of various problems. In a previous study (Brunzendorf & Meusinger 1999; hereafter paper 1), we have compiled an optical catalogue of galaxies in the inner 10 square degrees in order to investigate the morphological segregation and further statistical properties of the galaxies in this cluster. In the present paper, this catalogue is used to identify IRAS galaxies in the Perseus cluster in order to study their morphological properties and environment.

Send offprint requests to: H. Meusinger (meus@tls-tautenburg.de)

⋆ Visiting Astronomer, German-Spanish Astronomical Centre, Calar Alto, operated by the Max-Planck-Institute for Astronomy, Heidelberg, jointly with the Spanish National Comission for Astronomy

The influence of the environment on the evolution of global physical properties of galaxies is a matter of a longstanding debate (e.g., Schweizer 1976; Butcher & Oemler 1984; Dressler et al. 1994; Balogh et al. 1997; Ghigna et al. 1998; Abadi et al. 1999; Balogh et al. 1999; Hashimoto & Oemler 2000; Quilis et al. 2000). It is well known that encounters with nearby neighbours can induce both distortion and starbursts. In general, distorted galaxies were found to be more prevalent in regions with densities higher than the sparse field (Hashimoto & Oemler 2000). Slow tidal interactions occur in galaxy groups of low velocity dispersion (Couch et al. 1998) or in the peripheral lumps of clusters (Bothun & Schommer 1982), but are expected to be be rare within rich virialized environments (Ghigna et al. 1998). In dense cluster regions, tidal interactions with the cluster potential may be an important process that induces star formation activity and morphological distortion (Henriksen & Byrd 1996). On the other hand, various mechanisms may transform a star-forming galaxy to a passively evolving cluster galaxy or may even destroy a galaxy. Succesive high-speed encounters in the central cluster regions can lead to "galaxy harassment" (Moore et al. 1998; Fujita 1998; Caláneo-Roldán et al. 2000). Ram pressure and turbulent/viscous stripping by the hot intracluster gas may remove a large fraction of the gas reservoir and may, as a consequence, cease star formation in a galaxy that passes through the cluster centre (e.g., Gunn & Gott 1972; Bothun & Dressler 1986; Quilis et al. 2000). On the other hand, ram pressure may trigger starbursts due to the pressure increase in the interstellar medium of a galaxy that approaches the centre of the cluster (Dressler & Gunn 1983; Evrard 1991; Fujita & Nagashima 1999; Quilis et al. 2000). Galaxy harassment may trigger strong star formation activity as well (Fujita 1998). The radial distribution of cluster galaxies with enhanced star formation rates provides a constraint for the evaluation of the relative importance of these various processes. In this context, the population of blue cluster galaxies has been investigated in several studies (Abraham et al. 1996; Rakos et al. 1997; Balogh et al. 1997; Fujita 1998). Furthermore, the investigation of the spatial distribution of star-forming galaxies in large galaxy clusters (like Perseus) is important in the context of structure formation. The density of galaxies with active star formation in the outer parts of the clusters is related to the mass accretion rate of clusters at $z = 0$ and is therefore a direct probe of CDM theory.

Galaxies with enhanced star formation are well known to be emitters in the far infrared (FIR). The *Infrared Astronom-*

ical Satellite (IRAS) all-sky survey discovered a significant population of luminous infrared galaxies ($L_{\rm FIR} > 10^{11}\,L_\odot$; LIRGs) and ultra-luminous infrared galaxies ($L_{\rm FIR} > 10^{12}\,L_\odot$; ULIRGs) emitting a substantial, or even the dominant fraction of their bolometric luminosity in the FIR (Sanders & Mirabel 1996). One of the most fundamental properties of luminous IRAS galaxies is their distorted optical morphology (Joseph & Wright 1985; Clements et al. 1996b; Murphy et al. 1996; Rigopoulou et al. 1999). Clearly, the process of gravitational interactions plays a crucial role in triggering FIR activity of galaxies.

Both numerical studies (e.g., Noguchi & Ishibashi 1986; Noguchi 1990; Barnes & Hernquist 1996; Mihos & Hernquist 1996) and direct imaging of optically or FIR-selected galaxy samples (e.g., Sanders et al. 1986; Bushouse et al. 1988; Barton et al. 2000) have demonstrated that there exists a correlation between enhanced activity and morphological distortion as suggested by the classic papers by Toomre & Toomre (1972) and Larson & Tinsley (1978). The basic idea is that a distortion of the gravitational potential triggers dissipation of gas and/or cloud-cloud collisions and induces, therewith, star formation activity. On the other hand, the relation between interactions and star formation activity is complex, and there is a wide range of star-forming properties of interacting galaxies (e.g., Joseph et al. 1984; Bushouse 1986; Solomon & Sage 1988; Stein 1988; Hibbard & van Gorkom 1996). Morphological distortions are also common in samples of lower luminosity ($L_{\rm FIR} \leq 10^{11}\,L_\odot$) IRAS galaxies, though the distorted fraction seems to be less pronounced than for ULIRGs (e.g., Sanders et al. 1986; Leech et al. 1990; Lutz 1992; Klaas & Elsässer 1993).

The IRAS catalogue allows the construction of galaxy samples for the investigation of correlations between star formation activity, morphology and the environment where star formation is dynamically triggered. Yuan et al. (1996) have performed a deep optical identification of IRAS faint sources in the Virgo cluster. The present paper is concerned with IRAS sources identified with galaxies from the optical survey of the Perseus cluster region (paper 1). It has been recognised long ago that the Perseus cluster is remarkable in several aspects (see paper 1): it shows one of the highest velocity dispersion among the nearby clusters, a strong deficiency of spiral galaxies in the centre, a huge X-ray halo and a strong cooling flow. The total B-band luminosity of the Perseus cluster within the central 10 square degrees is about twice as high as for the Virgo cluster (paper 1), but Virgo is much nearer. This has implications for the luminosity range of IRAS galaxies that one is probing in the two environments. On the one hand, the distance of the Perseus cluster is small enough in order to expect the identification of a substantial number of IRAS galaxies. On the other hand, the distance is large enough to detect only the high-luminosity tail of the FIR luminosity function.

The plan of the paper is as follows: Sect. 2 describes the observational data and the evaluation of galaxy morphology. Correlations of photometric properties of the IRAS galaxies with morphology are discussed in Sect. 3. In Sect. 4, the morphological properties of the IRAS sample are compared with a control sample of optically selected "normal" galaxies and with the sample of apparently disturbed/interacting galaxies without IRAS detection. The environment is also discussed in Sect. 4. Conclusions are given in Sect. 5. Images and individual descriptions of the galaxies are presented in the Appendix.

2. Database and data reduction

2.1. The galaxy catalogue

The main source of optical data for the present study is provided by the catalogue of optical galaxies in the central region of the Perseus cluster (A 426) described in detail in paper 1. Throughout the present paper, galaxies are quoted with their numbers given in this catalogue. The catalogue contains accurate positions (better than $1''$), B_{25} magnitudes (better than 0.2 mag), major and minor axis of the 25 mag/$\Box''$ isophote, morphological types, and information on morphological peculiarities. The limiting magnitude of the catalogue is about 19.5; it is assumed to be complete down to $B_{25} \approx 18$ for galaxies with central surface brightness $\mu_B(0) < 23.2$ mag/$\Box''$.

The data given in the catalogue were derived from images obtained by the digital co-addition of a large number of Tautenburg Schmidt plates. The plates were taken in the B band, where recent star formation is indicated by the continuum radiation of young stars and stars of intermediate age (spectral types OBA). Extended structures can be traced down to $\mu_{\rm B} \approx 27$ mag/$\Box''$ on the stacked images. A detailed description of the plates and of the method of plate stacking is given in paper 1. For the purpose of an improved evaluation of faint structures indicative of tidal distortions, we have refined the method of digital coaddition (Meusinger et al. 1999; Froebrich & Meusinger 2000; Meusinger & Krieg, in preparation). The B images studied in the present paper were obtained from a new digital stacking of altogether 47 plates applying quality weighting factors and a "bad pixel" rejection algorithm. The method of quality weighting yields a further gain in limiting surface brightness of about 0.5 mag/$\Box''$ compared to the unweighted stacked image.

2.2. Galaxy selection

IRAS sources were selected both from the NED[1] and directly from the IRAS PSC. Due to the low galactic latitude of the field, the contamination by galactic sources is not neglegible. Therefore, we strictly consider only such indentifications with a small position difference relative to an IRAS source. (These differences are dominated by the IRAS position uncertainty and by the spatial extension of the galaxies.) The combination of the following three criteria is used to ensure a certain identification: (1.) the error ellipse for the IRAS position must overlap with the optical image, (2.) the difference Δ between the IRAS position and the optical centre of the galaxy must be less then $30''$ (approximately the mean IRAS position uncertainty in the field),

[1] The NASA/IPAC Extragalactic Database (NED) is operated by the Jet Propulsion Laboratory, California Institute of Technology, under contract with the National Aeronautics and Space Administration.

Table 1. Identified IRAS galaxies in the A 426 field.

no.	other	α	δ	$B_{25}(0)$	$v_{\rm r}$	IRAS desig.	Δ	$\log \frac{f_{60}}{f_{100}}$	$\log \frac{L_{60}}{L_\odot}$	$\log \frac{L_{\rm FIR}}{L_\odot}$	$\log \frac{L_{\rm FIR}}{L_{\rm B}}$
(1)	(2)	(3)	(4)	(5)	(6)	(7)	(8)	(9)	(10)	(11)	(12)
65	U 2608	03 15 01.4	42 02 09	13.6	6993	03117+4151	6	-0.19	10.82	10.83	0.58
94	U 2617	03 16 00.7	40 53 08	13.9	4860	03127+4042	11	-0.71	9.07	9.98	-0.15
95	U 2618	03 16 00.9	42 04 28	14.2	5385	03127+4153	5	-0.47	9.91	10.04	0.03
109	P 12166	03 16 34.4	41 02 50	15.4	4029	03132+4051	10	-0.41	9.81	9.91	0.38
121		03 16 45.8	40 19 48	15.6	4910	03134+4008	2	-0.42	10.04	10.15	0.70
140	N 1260	03 17 27.1	41 24 19	13.9	5631	03141+4113	5	-0.47	9.71	9.85	-0.28
199	U 2654	03 18 43.2	42 18 03	13.8	5793	03154+4207	7	-0.52	10.09	10.25	0.08
212	U 2659	03 18 53.3	40 35 45	14.2	6198	03156+4025	15	-0.54	9.84	10.01	0.00
270	N 1275	03 19 48.1	41 30 42	12.3	5264	03164+4119	1	-0.08	10.77	10.74	-0.03
342	P 12535	03 20 41.4	42 48 14	15.2	6770	03173+4237	28	≤ -0.51	9.66	≤ 9.82	≤ 0.21
383/384	I 316	03 21 19.9	41 55 50	:13.8	3000	03179+4145	6	-0.33	10.24	10.30	0.13
538	U 2718	03 24 43.7	41 58 09	14.5	6871	03213+4147	5	-0.42	10.08	10.18	0.29
540		03 24 49.2	41 04 24	16.5	22200	03214+4053	11	≤ -0.42	10.82	≤ 10.93	≤ 0.63
549		03 25 05.4	40 33 29	:15.5	7007	03217+4023	4	-0.21	10.79	10.80	1.31
552	U 2722	03 25 09.4	42 24 07	15.3	3574	03217+4213	10	-0.69	9.76	10.02	0.45
554	U 2724	03 25 13.0	40 41 53	:16.7	14308	03219+4031	17	≤ -0.01	10.86	≤ 10.81	≤ 0.97
571	U 2730	03 25 52.3	40 44 55	14.1	3772	03225+4034	20	-0.45	10.07	10.19	0.14
627	P 12933	03 28 27.8	40 09 16	13.9	4246	03251+3958	1	-0.24	10.63	10.65	0.52
658	N 1334	03 30 01.8	41 49 55	13.2	4237	03266+4139	2	-0.36	10.56	10.64	0.23

Column (1): number in the optical catalogue; Column (2): other name (N=NGC, I=IC, U=UGC, P=PGC), Columns (3),(4): optical position (J2000), Column (5): total magnitude of the part of the galaxy image brighter then 25 mag arcsec^{-2}, corrected for galactic foreground extinction and inclination (a colon marks uncertain values, mainly due to an overlapping object); Column (6): radial velocity in km sec^{-1}; Column (7): IRAS PSC designation; Column (8): distance in arcsec between the optical centre and the IRAS position; Columns (9)–(12): colours and luminosities derived from the colour-corrected flux densities from the IRAS PSC. In case of the systems 383/384, 540, 554 the optical data refer to the whole double or triple systems. Upper limit detections at 100 μm are indicated by $\leq$ in colons (9), (11), and (12).

and (3.) Δ must be less then the (inclination corrected) diameter of the 25 mag isophote of the B band image.

The 19 IRAS galaxies identified in this way are listed in Table 1. For the systems 540 and 554, the positions refer to the centre of the brightest galaxy in these groups. In the case of the extended interacting pair 383/384, the approximate centre of the system is given.

A few more IRAS sources were found close to the optical position of a galaxy, but not close enough for a certain identification. Among them is the radio head-tail galaxy IC 310 which has been identified with IRAS 03135+4108 in the NED. However, the position difference $\Delta = 70''$ is too large to include it in our sample. Moreover, the ULIRG IRAS 03158+4227 (Crawford et al. 1996; Murphy et al. 1996) is not included because the optical galaxy is too faint to be contained in our catalogue. With a redshift of $z = 0.134$, this source is much more distant than all other galaxies under consideration.

2.3. CCD observations

The 19 IRAS galaxies have been observed in the B band using the focal reductor camera CAFOS at the 2.2-m-telscope at Calar Alto, Spain, equipped with a SITe detector with pixel scale $0\farcs5$/pixel. The seeing was $1''$ to $1\farcs4$; typical exposure times were in the range of 1 000 to 2 000 s.

In addition, for most of the galaxies, CCD observations were taken in the redshifted Hα bands with the Tautenburg 2 m telescope in its Schmidt mode, equipped with a SITe chip with pixels of 24 μm side-length. Two interference filters of 100 Å band width were available, centred on 6673 Å or 6729 Å, respectively. For galaxies, where the redshift is too large, or where the redshifted Hα line does not perfectly fit into one of the two filter bands, an R band image was taken instead. The exposure times are typically about 3 000 s to 5 000 s with a minimum of 600 s for no. 627 and a maximum of 16 200 s for NGC 1275. The seeing was typically about $2''$.

HST WFPC2 images are available for the galaxies 65 and 270 from the HST archive.

2.4. Spectroscopy

Low-dispersion spectra of four IRAS galaxies from Table 1 have been obtained with CAFOS at the 2.2-m-telescope at Calar Alto. For the galaxies 342 and 540, the spectra were taken to measure redshifts (see paper 1). The galaxies 554 and 658 were observed to ensure that the bright nuclei are not pretended by the fortuitous superpositions of foreground stars. For all four galaxies, the spectra show prominent emission lines.

2.5. Optical photometry

The B-magnitudes listed in Table 1 are related to the 25 mag arcsec^{-2} isophote and were estimated as $B_{25}(0) = B_{25} - A_{\rm g} - A_{\rm i}$, where B_{25} is the apparent magnitude given in the catalogue, $A_{\rm g}$ is the galactic foreground extinction, and $A_{\rm i}$ is the correction for the inclination of the galaxy. We assume

Table 2. Morphological summary for the systems from Table 1: some questions addressed on optical morphology and environment.

no. (1)	type (2)	p/g (3)	nn (4)	i/m (5)	od (6)	bar (7)	ring (8)	knots (9)	sample (10)	remarks (11)
65	SBR	-	√	-	√	?	√	√	A	
94	SB	-	-	-	-	√	-	√	C	
95	S(BR?)	-	√	-	?	?	?	-	B	
109	S(comp)	-	-	-	-	-	?	-	C	
121	S(B?)	-	-	-	-	?	-	-	C	hi/f∗
140	SB/SB0?	√	-	?	-	?	-	-	B	
199	SBR	-	√	-	-	?	√	√	B	hi
212	S(B?)	-	-	-	-	-	-	?	C	hi
270	E(pec)/cD	-	√	?	√	-	-	√	A	
342	SBR	-	-	-	-	√	√	-	C	
383/384	S(B?)+S	√	-	√	√	√	-	√	A	
538	SB(R?)/Irr?	-	-	-	-	√	?	√	C	f∗?
540	S + S?	√	-	√	√	-	-	?	A	
549	Irr	-	-	√	√	-	-	-	A	f∗
552	S(pec)	-	-	?	?	?	?	-	B	
554	group	√	-	√	√	-	-	?	A	f∗?
571	S	-	-	-	-	-	-	(√)	C	hi
627	SB/Irr	-	-	?	√	?	-	?	A	f∗
658	SB(R?)	-	-	-	√	√	-	√	A	

$A_{\rm i} = \alpha(T) \log (a/b)$ with $\alpha = 0$ mag for ellipticals and 0.8 mag for spirals, respectively, (e.g. Cunow 1992), a, b are the major and minor axis, respectively, of the 25 mag isophote. No inclination correction is applied for the systems 383/384 and 554 because of their complex structure. For 540, only the brighter galaxy is corrected, which is probably an inclined spiral. Galactic extinction values $A_{\rm g}$ were taken from the NED.

2.6. Optical morphology

B band images of the 19 galaxies from Table 1 are shown in Appendix A along with brief individual descriptions of the galaxies. Morphological properties are summarized in Table 2. Morphological types (column 2) were taken from the catalogue. Column 3 indicates the presence of nearby galaxies of comparable magnitude with signs for physical connection (light bridges, common halos, tidal structures), i.e. physical pairs or groups (p/g). Less strong indications (in the statistical sense) for interactions are provided either by fainter ($\Delta B \gtrsim 3$) companions or by nearby neighbours (nn) of comparable magnitude but without clear-cut signs for physical connection (column 4). Direct evidence for interaction or merging (i/m) is marked in column 5. Systems with obviously disturbed (od) morphology are classified in column 6. Further, the appearance of a bar, of ring structures, and of bright blue knots are checked in columns 7 to 9. In column 10, the galaxies are binned into 3 samples according to the strength of their morphological disturbance (see below). Remarks in Column 11 refer to a nearby or superimposed foreground star (f∗) or to a highly inclined system (hi).

The procedure of evaluating morphology is outlined in detail in paper 1. It seems impossible to capture the whole range of morphological peculiarities with a simple classification scheme. Roughly speaking, morphological distortions are characterized in particular by strong deviations from symmetry and/or by the existence of close companions (e.g., Hashimoto & Oemler 2000). Specific manifestations of asymmetric light distributions include tidal tails and plumes, unusual spiral structure (e.g., three-armed, M 51-type), or spheroidal components with non-regular, non-concentric, or non-elliptical isophotes. Moreover, interactions can result in quite symmetric polar ring structures as well (Theys & Spiegel 1977; Whitmore et al. 1990; Bekki 1998). On the other hand, axisymmetric galaxies with a regular elliptical bulge and with a thin, circular and obviously planar disk are considered as "normal".

In the present study, it is our main aim to distinguish between disturbed galaxies and undisturbed, "normal" galaxies. Such an attempt can not be completely objective, and it must be emphasized that quantifying peculiarities still remains a challenge. Our classification is based on the visual impression of the strength of morphological peculiarities on a scale corresponding to a substantial fraction of a galaxy. For this goal, we primarily evaluate the homogeneous set of the B band images.

To study correlations between FIR activity and morphological disturbance, we define three subsamples (Table 2):

- subsample **A**: the 8 galaxies with obviously distorted morphology (o/d in column 6);
- subsample **B**: 4 galaxies, where either weak indications for distortions are found (95, 552), or no such indications are found, but the galaxies either belong to a close pair (140) or have nearby neighbours (199).
- subsample **C**: 7 galaxies with rather "normal" morphology. For 4 of the 7 galaxies, the visual inspection is hampered by either the high inclination of the galaxy or by a nearby star. Thus, weak indications for distortions may be hidden.

2.7. Infrared fluxes and luminosities

Flux densities f at 12, 25, 60, and 100 μm where taken from the IRAS PSC. Only for a few galaxies in the sample, the 12 μm and the 25 μm flux densities are above limit detections. In the following, we shall consider therefore only luminosities and colours related to the 60 and 100 μm bands. The 60 μm flux density is better than limit detections for all galaxies, and only three galaxies have f_{100} detections of low quality. With the possible exceptions of IRAS 03127+4042 and IRAS 03217+4213, there is no source in the sample indicating a probable contamination by galactic "cirrus" (i.e., $\log f_{60}/f_{100} < -0.7$; Clements et al. 1996a).

As an alternative database, we also consider the flux densities at 60 and 100 μm derived by Wise et al. (1993) for 98 sources within one Abell radius (i.e., 97′) of A 426 with improved sensitivity compared to the PSC. The differences in the flux densities between the data from the PSC and from Wise et al. are typically 10–20% at 60 μm and 30–40% at 100 μm. We identified only 12 galaxies from the optical catalogue with IRAS sources for which both f_{60} and f_{100} are given by Wise et al. (1993).

The flux densities have been colour-corrected assuming thermal spectral energy distributions for all galaxies. The FIR luminosity is calculated exclusively from the flux densities at 60 μm and 100 μm using the FIR flux $F_{FIR} = 1.26\,10^{-14}(2.58 f_{60} + f_{100})$, where the flux densities f_ν are in Jy and the flux F is in W m^{-2} (Fullmer & Lonsdale 1989). In addition, also the monochromatic luminosity at 60 μm, L_{60}, is computed. For all cluster galaxies we assume a distance of 74 Mpc. For the background galaxies, a Hubble constant $H_0 = 75$ km s^{-1} Mpc^{-1} is adopted.

The ratio of the FIR to optical (blue) luminosity is calculated from $L_{\rm FIR}/L_{\rm B} = F_{\rm FIR}/F_{\rm B}$ adopting $F_B = \nu f_\nu(0.44\,\mu{\rm m})$=$2.88\,10^{-8}\,10^{-0.4\,B_T(0)}$, where $B_T(0)$ is the total B magnitude corrected for foreground extinction and inclination. We assume $B_T(0) = B_{25}(0)$, as the correction for the transformation $B_{25} \rightarrow B_T$ is smaller then the other corrections for the calculation of $B_T(0)$. Since the IRAS fluxes are not clearly attributed to one of the galaxies in the systems 383/384, 540, and 554, the $B_{25}(0)$ magnitude of the whole system is used in these cases. The results are listed in Table 1 for the flux densities from the IRAS PSC.

With the completeness limits of the IRAS PSC, $f_{60,\rm lim} = 0.5$ Jy and $f_{100,\rm lim} = 1.5$ Jy, we expect to find preferably galaxies with $\log L_{60}/L_\odot > 9.64$ and $\log L_{\rm FIR}/L_\odot > 9.8$ at the distance of A 426. This is in perfect agreement with the data in Table 1. The mean values for the whole sample from Table 1 are $\langle \log L_{\rm FIR}/L_\odot \rangle = 10.26 \pm 0.37$ and $\langle \log L_{\rm FIR}/L_{\rm B} \rangle = 0.34 \pm 0.43$.

3. Properties of the IRAS galaxy sample

3.1. Cluster membership

Radial velocities have been available from the NED or the PGC, respectively, for 17 of the 19 systems in Table 1. For the galaxies 342 and 540, radial velocities were obtained for the present study with CAFOS at the 2.2 m telescope on Calar Alto, Spain (see paper 1). Cluster membership is checked by the radial velocity criterion outlined in Kent & Sargent (1983). With the exception of 540 and 554, which are clearly in the background, the radial velocity data are consistent with cluster membership (Fig. 1). We assume that all galaxies from Table 1 are members of the Perseus cluster, with the exceptions of 540 and 554.

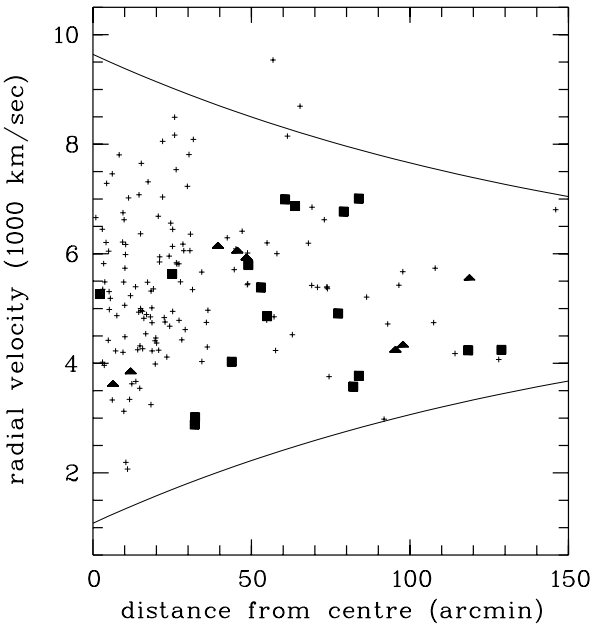

Fig. 1. The heliocentric radial velocity versus projected cluster centre distance for the catalogued galaxies (plus signs). The IRAS galaxies (without galaxies 540 and 554 which have $cz \geq 10\,000$ km s^{-1}) are plotted as filled squares, peculiar galaxies discussed in Sect. 4 as triangles. The lines correspond to the cluster membership demarcation as discussed by Kent & Sargent (1983).

3.2. FIR colours, FIR excess and morphological peculiarity

The mean values of the FIR colour index $\log f_{60}/f_{100}$, the FIR luminosity, and the FIR excess are listed in Table 3 for our three morphological subsamples. The results are illustrated by Figs. 2 and 3. Fig. 2 exhibits a correlation between the FIR luminosity and $\log f_{60}/f_{100}$. Such a trend is expected in models of thermal dust emission where a stronger energy input into the interstellar medium leads both to a stronger heating of the dust and to higher FIR luminosity and FIR excess (see Sanders & Mirabel 1996). For galaxies in the IRAS Bright Galaxy Survey (Soifer et al. 1986), the mean f_{60}/f_{100} ratio increases with increasing FIR luminosity, with $\log f_{60}/f_{100} > -0.3$ for ULIRGs (Soifer & Neugebauer 1991; Sanders et al. 1995). This colour criterion has been used by Kim & Sanders (1998) for the selection of ULIRGs in the 1 Jy survey. There are five galaxies in our sample with $\log f_{60}/f_{100} > -0.3$. All five belong to the "interaction group" **A**.

On the basis of Fig. 2, the sample of galaxies may be divided into two subsamples, one at the lower left and the other one at

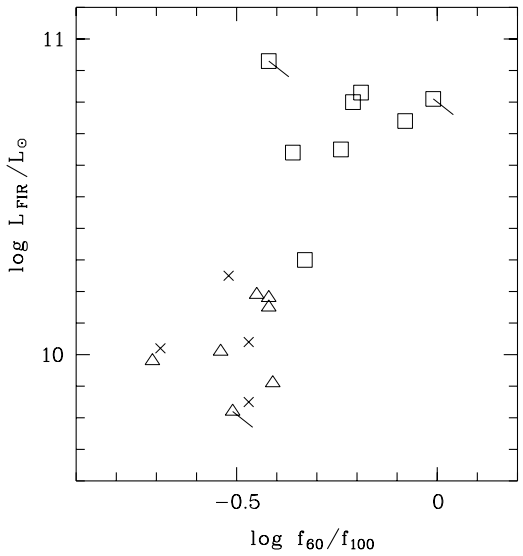

Fig. 2. FIR luminosity versus the 60-to-100 μm colour. (Open squares: subsample **A**, crosses: subsample **B**, open triangles: subsample **C**). For IRAS sources with only upper limit detections at 100 μm the direction of the shift is indicated.

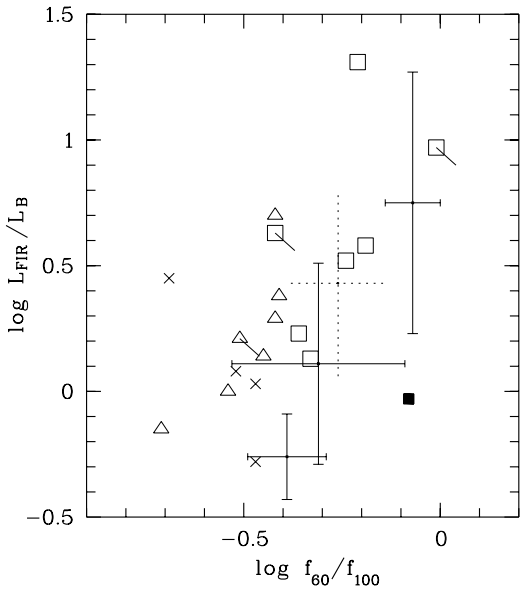

Fig. 3. Ratio of FIR luminosity to visual (B band) luminosity versus the 60-to-100 μm colour. The cD galaxy NGC 1275 is marked by the filled square; all other symbols as in Fig. 2. For comparison, the mean values and standard deviations for the subsamples of (a) isolated galaxies, (b) pairs, and (c) mergers (bottom to top) from the list of galaxies given by Young et al. (1996) are shown as error crosses. The corresponding values for a comparison sample of starburst galaxies from Coziol et al. (1998) are shown by the dotted error cross.

the upper right of the diagram, with the merger 383/384 near the dividing line. This sampling correlates very well with the sampling from the optical morphology: all galaxies in the upper right group have been classified as morphologically distorted (subsample **A**), whereas the galaxies in the lower left part belong to the subsamples **B** and **C** without any difference between **B** and **C**. A similar result is found when the FIR excess is plotted against $\log f_{60}/f_{100}$ (Fig. 3). The weak trend of increasing FIR excess with increasing f_{60}/f_{100} (Fig. 3) is known from other data (Soifer et al. 1987 and references therein; Leggett et al. 1987; Yuan et al. 1996) and is expected for FIR luminosity due to thermal dust emission (see Sanders & Mirabel 1996). Furthermore, we find also a weak correlation of the FIR excess with $L_{\rm FIR}$ (with the exception of NGC 1275, which is a cD galaxy with a variable Seyfert nucleus).

Table 3. Sample-averaged values for the three morphological subsamples from Table 2. The values in the bottom line of each item refer to the list and flux densities from Wise at al. (1993).

subsample	**A**	**B**	**C**
distortion/ interaction	yes	?	no
number of galaxies	8 5	4 2	7 5
$\langle\log f_{60}/f_{100}\rangle$	-0.23 ± 0.14 -0.34 ± 0.19	-0.54 ± 0.10 -0.76 ± 0.04	-0.49 ± 0.11 -0.79 ± 0.21
$\langle\log L_{\rm FIR}/L_{\rm B}\rangle$	0.54 ± 0.44 0.65 ± 0.57	0.07 ± 0.30 0.10 ± 0.31	0.22 ± 0.27 0.46 ± 0.25
$\langle\log L_{60}/L_{\odot}\rangle$	10.69 ± 0.21 10.67 ± 0.27	9.87 ± 0.18 9.94 ± 0.32	9.89 ± 0.18 10.01 ± 0.13
$\langle\log L_{\rm FIR}/L_{\odot}\rangle$	10.71 ± 0.19 10.75 ± 0.22	10.04 ± 0.16 10.25 ± 0.32	10.03 ± 0.14 10.35 ± 0.23
$\langle\Psi/{\rm M}_{\odot}yr^{-1}\rangle$	63 ± 23 64 ± 28	10 ± 4 12 ± 8	10 ± 4 12 ± 4
$\langle T_d/{\rm K}\rangle$	38 ± 5 35 ± 5	30 ± 2 25 ± 1	30 ± 2 25 ± 3
$\langle\log m_d/{\rm M}_{\odot}\rangle$	6.60 ± 0.32 6.87 ± 0.35	6.56 ± 0.27 7.19 ± 0.42	6.46 ± 0.21 7.33 ± 0.59

We compare the results from Table 3 with the corresponding mean values for the subsamples of (a) isolated galaxies, (b) pairs, and (c) mergers from the galaxy sample studied by Young et al. (1996). For the sake of comparison, we exclude from the Young et al. sample all galaxies with $\log L_{\rm FIR}/L_{\odot} < 9.5$ to minimize a luminosity-based selection bias. The results (Fig. 3) show qualitatively similar trends as our date from Table 3. The FIR properties make our subsample **A** comparable with a mixture of mergers and pairs from the Young et al. (1996) sample. The mean values derived for a comparison sample of 144 IRAS starburst galaxies with $9.8 < \log L_{\rm FIR}/L_{\odot} \leq 11.0$ (i.e., a range comparable with our sample) from the Pico dos Dias survey (Coziol et al. 1998) are also in good agreement with our subsample **A** (Fig. 3). The FIR excess from subsample **C** is significantly higher than for normal isolated galaxies from Young et al. (1996).

3.3. Derived properties: star formation rate, dust mass, dust temperature

It is expected that the FIR emission is an efficient tracer of dust in galaxies. We estimate dust masses from the relation given by Thuan & Sauvage (1992) which is based on the assumption

that the total mass of dust is proportional to the flux density at 100 μm. Furthermore, dust temperatures $T_{\rm d}$ are calculated from the FIR colour index $\log f_{60}/f_{100}$ assuming a Planck-function and a λ^{-1} emissivity law. FIR emission is generally assumed to originate from three distinct components (Rowan-Robinson & Crawford 1989): the disk component with $T_{\rm d} \approx 20$ K, a starburst component with $T_{\rm d} \approx 30$–60 K, and a Seyfert component with $T_{\rm d} \approx 200$ K. The estimated mean values of the dust temperatures for the subsamples (Table 3) indicate the presence of starburst components. The strength of the starbursts increases with the strength of the morphological distortion.

If heating of dust is dominated by stellar radiation, the FIR emission of galaxies can be used as a tracer of the population of massive stars. To estimate the star formation rate (SFR), we adopt the simple relation given by Clements et al. (1996a), which is based on the 60 μm flux and on a normal IMF between 0.1 $M_\odot$ and 60 $M_\odot$. The results show a correlation of $T_{\rm d}$ with the SFR (Fig. 4); no correlation is seen between the dust mass and the SFR. Mean values of SFR, dust mass, and dust temperature for the three subsamples are given in Table 3.

The relation between the global SFR and the FIR emission is still controversial (Kennicutt 1998, and references therein). In particular, the emission of a cooler component (cirrus) heated by the general stellar radiation field may play a significant role in the disks of early type galaxies. Thus the SFR may be overestimated when a relation derived for starburst galaxies is applied to "normal" galaxies. Furthermore, the estimated SFRs strongly depend on the IMF. For instance, a lower mass limit of 8 $M_\odot$, instead of 0.1 $M_\odot$, would reduce the SFR by a factor of 6 (see Clements et al. 1996a). The observations of the most massive stars in starburst galaxies are consistent with the classical Salpeter IMF, whereas the situation is much more uncertain for low-mass stars. In particular, there is evidence for top-heavy IMFs in some starburst galaxies (see Leitherer 1998, and references therein). It should be noted that the SFRs of about 5 to 15 $M_\odot$ yr^{-1} estimated for the galaxies in subsample **C** are not much larger than the typical SFR derived by Kennicutt (1998, his Table 1) for spiral galaxies.

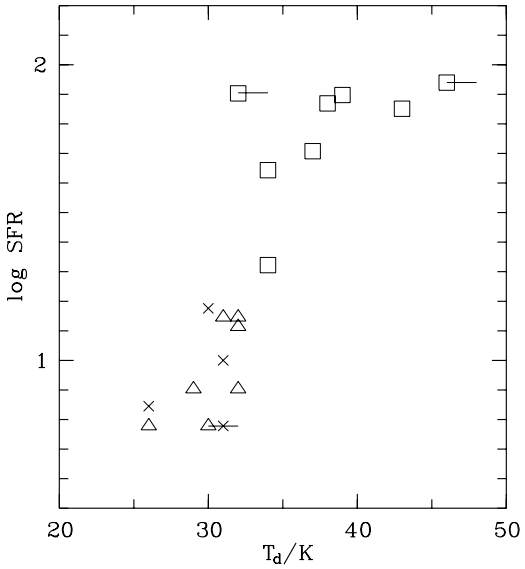

Fig. 4. Star formation rate (in $M_\odot$ yr^{-1}) versus dust temperature T_d. Symbols as in Fig. 2.

4. Comparison of the IRAS sample and the whole galaxy sample

4.1. Fraction of disturbed/interacting galaxies

To evaluate the fraction of disturbed/interacting galaxies among the IRAS sources, we define a control sample of galaxies with a similar range of magnitudes and morphological types on the basis of the whole galaxy sample. We use the counting convention from paper 1 and consider only galaxies with a probability for S or Irr larger than 50% and with $B_{25} \leq 16.5$. The control sample contains 66 galaxies. Among them are 7 distorted non-IRAS galaxies and 5 (subsamples **A**) or 12 (subsamples **A+B**) distorted IRAS cluster galaxies, respectively, i.e. a "disturbance fraction" between 18% and 29% for the whole sample. With 31% to 56%, respectively, the corresponding fraction is considerably larger in the IRAS sample than in the control sample. These results support the picture that gravitational interactions trigger not only super-starbursts in ULIRGs but also moderate starbursts in FIR galaxies of lower luminosity.

On the other hand, there are galaxies in the optical catalogue which were not identified as FIR active galaxies but which do show morphological distortions. In order to check the relevance of this fact, the images of all 660 galaxies were inspected again to select systems with clear-cut evidence for distortions (strong morphological peculiarities, tidal tails, polar rings, nearby neighbours with small velocity difference and/or distorted morphology). We find 14 such systems among the galaxies with $B < 17$ and $a_{25} \geq 15''$. It seems very unlikely that a substantial fraction of these galaxies are misclassified, e.g. due to the random superposition of galaxies along the line of sight. Radial velocities are available only for 8 of these 14 galaxies. On the basis of the radial velocity versus cluster centre distance diagram (Fig. 1), all these 8 galaxies are considered as cluster members.

None of these galaxies is identified with an IRAS source. We performed Monte Carlo-simulations to check whether the non-detection by IRAS can be simply due to the IRAS detection limit in combination with the fact that the mean B-luminosity $\langle \log L_{\rm B}/L_\odot \rangle = 9.59$ of this sample is lower than $\langle \log L_{\rm B}/L_\odot \rangle = 9.92$ for the IRAS sample. The simulations use the measured $L_{\rm B}$ along with an adopted FIR excess to compute the distribution of $L_{\rm FIR}$ for the sample of disturbed non-IRAS galaxies. Adopting $\langle \log L_{\rm FIR}/L_{\rm B} \rangle \pm \sigma = 0.34 \pm 0.43$ from our whole IRAS sample, we expect 8 galaxies to be contained in the PSC. Even if the FIR excess of normal IRAS galaxies is adopted, 6 galaxies should have been detected. For FIR properties similar to subsample **A**, 11 galaxies are expected to show FIR luminosities brighter than the IRAS detection limit.

The fact that there are approximately as many distorted non-IRAS galaxies as IRAS galaxies with similar morphology obviously means that peculiarities in themselves do not necessarily

indicate elevated star formation. The impact of gravitational disturbance on the star formation activity depends on the details of the interaction geometry and different timescales for the starburst and for the persistence of the distortion (e.g., Hibbard & van Gorkom 1996). However, the most important aspect is certainly the gas content of the involved galaxies. In this context, rapid gas stripping in the harsh conditions near the cluster centre may be a crucial process. It is tempting to interpret the distorted non-IRAS systems as galaxies which have already passed the cluster core and have lost most of their gas, whereas the stellar orbits have not been affected much yet by processes like harassment.

Using the morphological information given in the catalogue (see paper 1), we find a fraction of 45% of the galaxies in the control sample to show indications for a central bar. For the late-type IRAS cluster galaxies the fraction amounts to 60%. The fraction of ring structures among the IRAS galaxies is about 30%, compared to 17% for the comparison sample. These numbers seem to indicate differences in the sense that both bar-like and ring-like structures are more abundant in FIR active galaxies than in normal spirals.

4.2. Discussion of the environment

A plot of the positions on the sky of all galaxies from the optical catalogue is shown in Fig. 5. The concentration of the brighter galaxies ($B_{25} < 17$) towards the cluster centre is evident. The projected distribution of the IRAS galaxies, on the other hand, is considerably less concentrated. With the exception of the central dominant cluster galaxy NGC 1275, IRAS galaxies seem to populate preferentially the outer cluster regions of lower density.

In order to verify this impression, we consider the distribution of the fraction f of IRAS galaxies as a function of the cluster-centric radius r, the local galaxy number density μ, and the local B-band luminosity density $l_{\rm B}$ (Fig. 6). A clear trend is indicated if the fraction f of IRAS galaxies among the brighter galaxies is considered (Fig. 6, top). This trend may reflect the well-known (paper 1) morphological segregation, i.e. the relative underabundance of (gas-rich) late-type galaxies in the central cluster region. Indeed, the trend is less pronounced if the fraction f of the IRAS galaxies among the late-type galaxies only is considered (Fig. 6, bottom). The distribution of the distorted non-IRAS galaxies shows a similar trend, but the deviation from the distribution of the bright galaxies is less pronounced and the number ratio of distorted non-IRAS galaxies to late-type galaxies does not show a clear dependence on density or distance from centre.

Of course, the galaxy samples under discussion are quite small, and the formal statistical errors are considerably large. In Fig. 6, the binning was chosen in such a way that there are typically 3 to 8 peculiar galaxies (IRAS or distorted non-IRAS, respectively) per bin. The corresponding counting errors (assuming Poisson statistics) yield formal relative errors $\Delta f/f$ of typically 0.4 to 0.6. To check the significance of the trends indicated in Fig. 6, we applied a Spearman rank-correlation test (e.g., Siegel & Castellan 1988). This allows a robust, nonparametric test of the null hypothesis that there is no correlation ($C \approx 0$) between f and r, μ, or $l_{\rm B}$, respectively. On a chosen significance $\alpha = 0.05$, the null hypothesis $H_0 : C \approx 0$ has to be rejected clearly for the IRAS galaxies in panels **a** to **e**. For the distorted non-IRAS galaxies, on the other hand, $H_0 : C \approx 0$ is accepted for the distributions shown in panels **a,d,e,f**. A similar result is found when the significance of the correlations is tested by Kendall's tau.

Despite the central dominant galaxy NGC 1275, there are two further peculiar galaxies found in the immediate central region of the Perseus cluster: the non-IRAS galaxies 225 and 321. The velocities relative to the cluster centre are $\Delta v = 1\,600$ km s^{-1} and 1 400 km s^{-1}, respectively. These galaxies are perhaps interesting candidates for beginning galaxy harassment. A more detailed discussion of these systems is beyond the scope of the present paper.

5. Conclusions

We have identified 19 IRAS PSC sources with catalogued optical galaxies ($B_{25} \lesssim 19.5$) in a 10 square degree region around the centre of the rich galaxy cluster A 426 (Perseus). Based on radial velocity data, 17 of these galaxies are considered as cluster members.

Both the FIR luminosity and the FIR excess are found to be correlated with the colour index $\log f_{60}/f_{100}$, as is expected for thermal dust emission due to starbursts (cf. Sanders & Mirabel 1996). The global SFRs derived from the 60 μm luminosity, indicate moderate starbursts, at least for a significant fraction of the sample. The SFR is correlated with the dust temperature obtained from the 60-to-100 μm colour.

Similar correlations have been found by Yuan et al. (1996). These authors have identified a large sample of 276 IRAS galaxies on UKST plates of a 102 square degree field in the Virgo cluster area to a magnitude limit of $B \approx 22$. Yuan et al. report an anticorrelation between $\log f_{100}/f_{60}$ and the FIR excess for the 199 galaxies with moderate- or high-quality detections at both 60 and 100 μm and a weak correlation between the infrared excess and the infrared luminosity for the 83 probable cluster members. Most of the IRAS galaxies in the Virgo sample are IR-normal spirals (though Yuan et al. state that it is difficult to classify the faint galaxies by morphological structure) having $\log L_{\rm FIR}/L_{\rm B} < 0$ and $\log L_{\rm FIR}/L_{\odot} < 9$. Compared with the Virgo IRAS galaxies, our sample in the Perseus field is stronger biased towards the high-luminosity tail of the FIR luminosity function (mean values $\langle \log L_{\rm FIR}/L_{\rm B} \rangle = 0.34 \pm 0.43$ and $\langle \log L_{\rm FIR}/L_{\odot} \rangle = 10.26 \pm 0.37$).

We find a trend for higher FIR activity, and therewith higher SFRs, to occur in systems with stronger signs of gravitational distortions than in rather "normal" systems. The fraction of distorted galaxies among the IRAS sample is significantly higher than for a comparison sample of galaxies from the optical catalogue. This supports the view that enhanced star formation activity of galaxies is related to morphological distortions. On the other hand, the number of distorted galaxies which were not

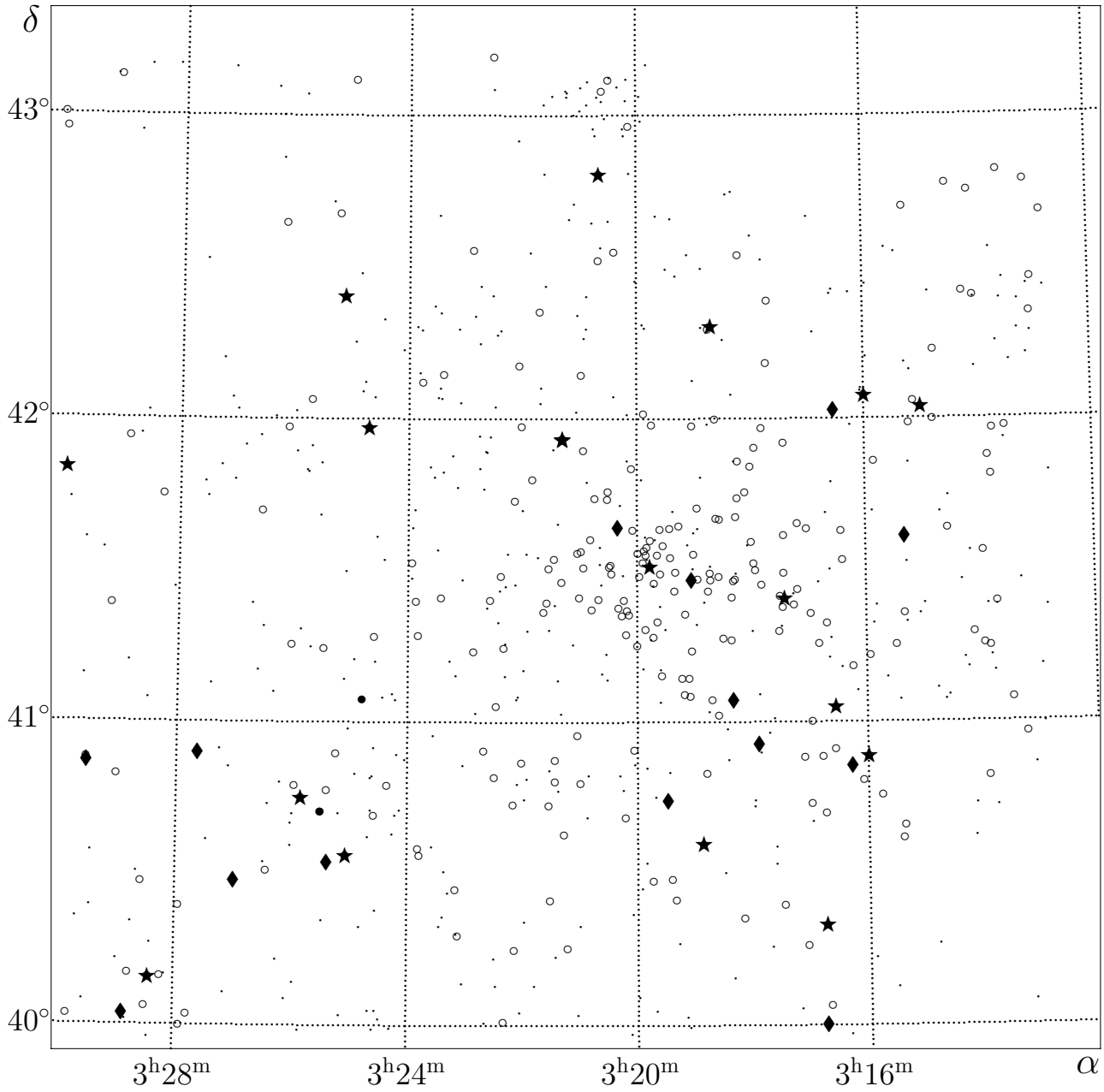

Fig. 5. Positions (J 2000.0) of IRAS galaxies (big stars for cluster members and bullets for background galaxies) and interacting/disturbed non-IRAS galaxies (black lozenges) from the present study, compared with the distribution of the galaxies with $B < 17$ (open circles) and the fainter galaxies (dots) from the catalogue. (The void in the upper right corner is due to the calibration wedge on the Schmidt plates.)

detected by IRAS is comparable with the number of distorted IRAS galaxies. Disturbed optical morphology does, of course, not guarantee enhanced star formation.

The spatial distribution of the IRAS galaxies in the Perseus field is less strongly concentrated towards the high-density region in the cluster centre than the cluster galaxies in general, and even less strongly than the late-type galaxies. This trend is less pronounced for the distorted non-IRAS galaxies. It is tempting to speculate that these differences are related to the rapid stripping of gas in the cluster environment. Only galaxies which have just entered the cluster still have their gas reservoir and may become IRAS galaxies (perhaps after the SFR has been elevated by external triggers). When a galaxy has reached the centre even on its first passage, it may have lost all its gas and cannot become an IRAS galaxy. As the timescale for galaxy harassment is longer than the gas stripping timescale, distorted non-IRAS galaxies can be observed near the cluster centre on the first or maybe second passage.

It would be very useful to obtain optical colours for the galaxies discussed in the present study and for a representative sample of Perseus galaxies. The comparison of the colours for the various samples will provide additional constraints for the

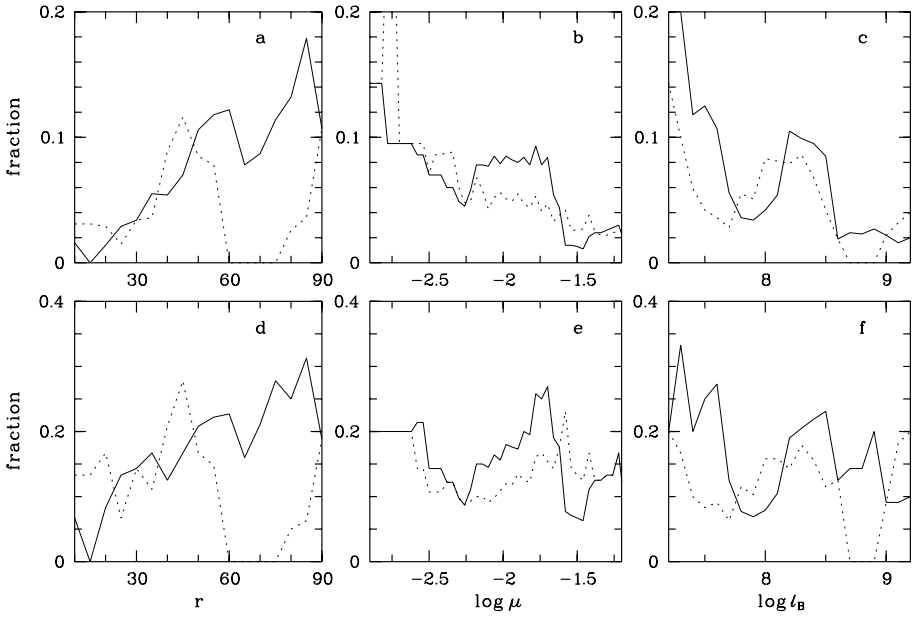

Fig. 6a–f. Distribution of the fraction of the IRAS cluster galaxies (solid line) and of the distorted non-IRAS galaxies (dotted line), respectively, as a function of **a,d** the distance r from the cluster centre (arcmin), **b,e** the projected number surface density of galaxies (number per square arcmin), and **c,f** the B band luminosity density $l_{\rm B}$ ($L_\odot$ per square arcmin). In the upper row, the fraction is related to all catalogued galaxies with $B_{25} \leq 17$, in the bottom row to the catalogued late-type galaxies with $B_{25} \leq 17$ only. The surface densities are related to all galaxies with $B_{25} \leq 17$ and were averaged over the circular areas with radius $15'$ around each galaxy. For the cluster centre (NGC 1275), we have $r = 0, \log \mu = -1.19, \log l_{\rm B} = 9.18$.

interpretation of the evolutionary status of the IRAS galaxies and of the morphologically distorted galaxies in the Perseus cluster.

Acknowledgements. This research is based on observations made with the 2.2 m telescope of the German-Spanish Astronomical Centre, Calar Alto, Spain. This research is partially based on data from the HST archive. The research has made use of the NASA/IPAC Extragalactic Database (NED) which is operated by the Jet Propulsion Laboratory, California Institute of Technology, under contract with the National Aeronautics and Space Administration. The referee, Neil Trentham, is acknowledged for his constructive criticism.

Appendix A: individual descriptions of the IRAS galaxies

65 The optical image of UGC 2608 is dominated by a bright nucleus within a bright bar. The bar is surrounded by a non-concentric, irregular ring structure which appears strongly disturbed in SE and shows pronounced bright Hα knots in N and E and faint outer filaments in NW. The HST WFPC2 image clearly reveals a patchy, two-armed spiral structure inside the bar. There are several nearby neighbours, including no.60 (IC 301, $\Delta\, B = 0.3$, separation $11.5'$, $\Delta v = 143\,\mathrm{km\,s^{-1}}$) and no. 67 ($\Delta\, B = 2.1$, separation $1.5'$). UGC 2608 is classified as a Seyfert 2 (Hewitt & Burbidge 1991) and as an ultraviolet excess galaxy (= Mkn 1073). It is also known both as an X-ray source with a thermal (?) spectrum (Rhee et al. 1994) and as a radio source at several frequencies. The galaxy is one of the 20 starburst galaxies with the highest 4.85 GHz luminosities from the survey by Condon et al. (1991). A high resolution VLA map at 1.425 GHz is shown by Condon et al. (1996); for near infrared images see Smith et al. (1996). The low-resolution K-band spectrum (Smith et al. 1996) shows strong Br$\,\gamma$ and H_2 emission.

94 A big spiral with open arms. There is perhaps a small bar. The spiral structure seems slightly disturbed: the arm developping from the center to NW splits up in several parts. In S, the outer arm is kinked. Several exceptionally bright knots in the arms.

95 A big, warped spiral, perhaps barred and with inner ring structure and unusual dust absorption. Northern isophotes are slightly elongated toward the nearby ($1'$) neighbour no. 96 ($\Delta\, B = 3$). Several fainter galaxies nearby.

109 A very compact, small galaxy. The outer isophotes are slightly non-concentric. Inner ring or tightly wound spiral structure.

121 A highly inclined spiral with bright inner arms (and perhaps a bar). A bright knot N of the core.

140 In the PGC, this galaxy is classified as "L". We found weak indications for outer spiral structure. Both the profile and the isophote analysis indicate a bar. There is a faint light bridge towards the ringed galaxy 147 (distance $1'$, $\Delta\, B = 2$, $\Delta v \approx 300\,\mathrm{km\,s^{-1}}$).

199 The rather irregular appearance of this galaxy is best explained assuming a bright inner ring structure with bright knots and strong dust absortion. A faint arc about $50''$ S of the centre is probably part of an outer spiral arm. Three galaxies are within about $2r_{25}$ (204,206, anonymous). The galaxy has been detected as a radio source (Gisler & Miley 1979) and as a $ROSAT$ X-ray source with thermal (?) spectrum (Rhee et al. 1994).

212 An inclined late-type spiral without any sign for distortion.

270 NGC 1275, the central galaxy of A 426, is well known as a very peculiar object in the centre of a strong cooling flow, with a Seyfert nucleus (Hewitt & Burbidge 1991; Boisson et al. 2000). The galaxy has a cD envelope with many H$\,\alpha$ filaments, an F-type optical spectrum, and young globular clusters. It is detected as a radio source at many frequencies and as an X-ray source with complex structure. The filamentary structure associated with many bright knots is clearly seen in our Hα

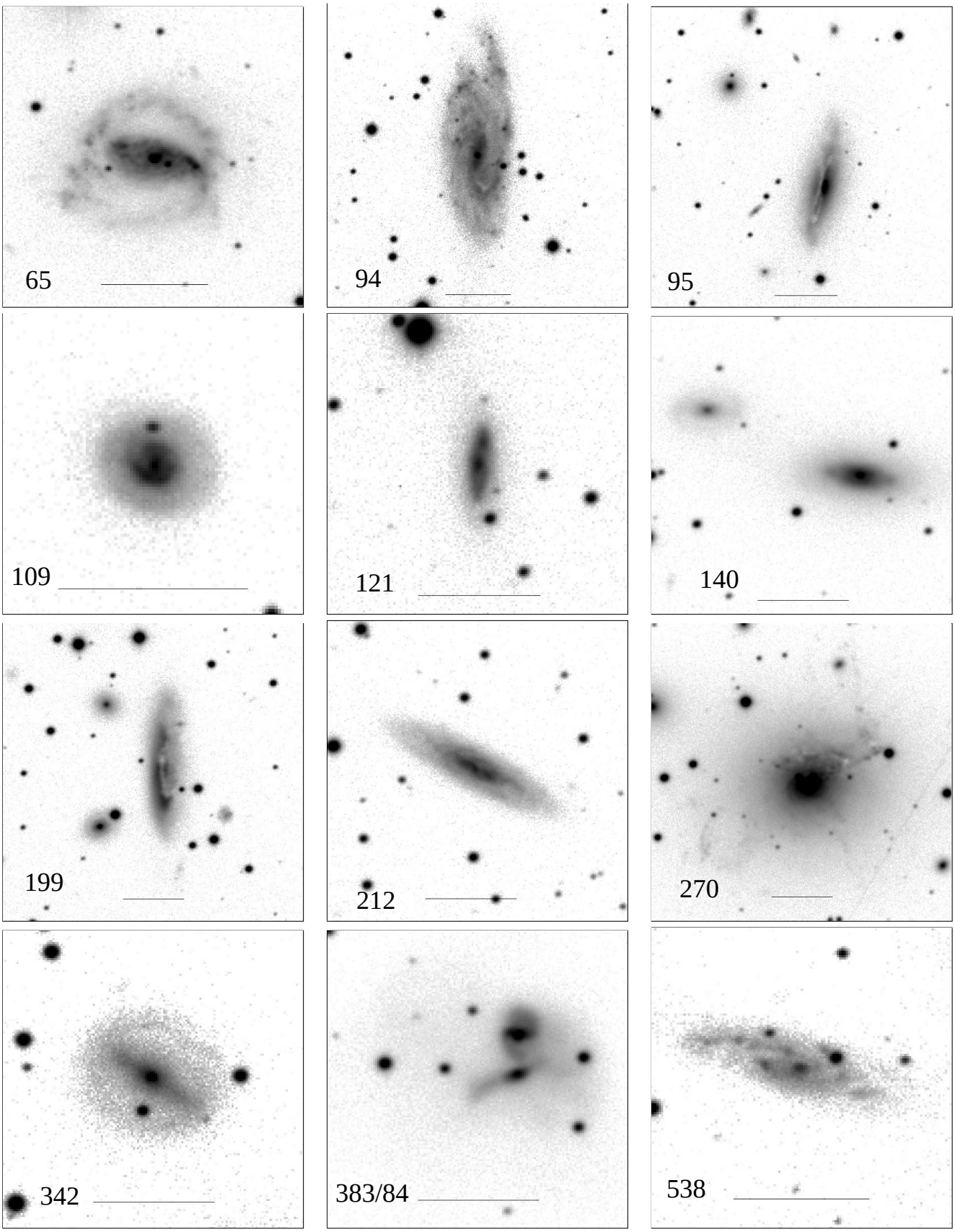

Fig. A.1. CCD images in the B band of the IRAS galaxies in the Perseus cluster field. North is up, east is to the left. The catalogue numbers of the galaxies are given. The horizontal bars correspond to $30''$.

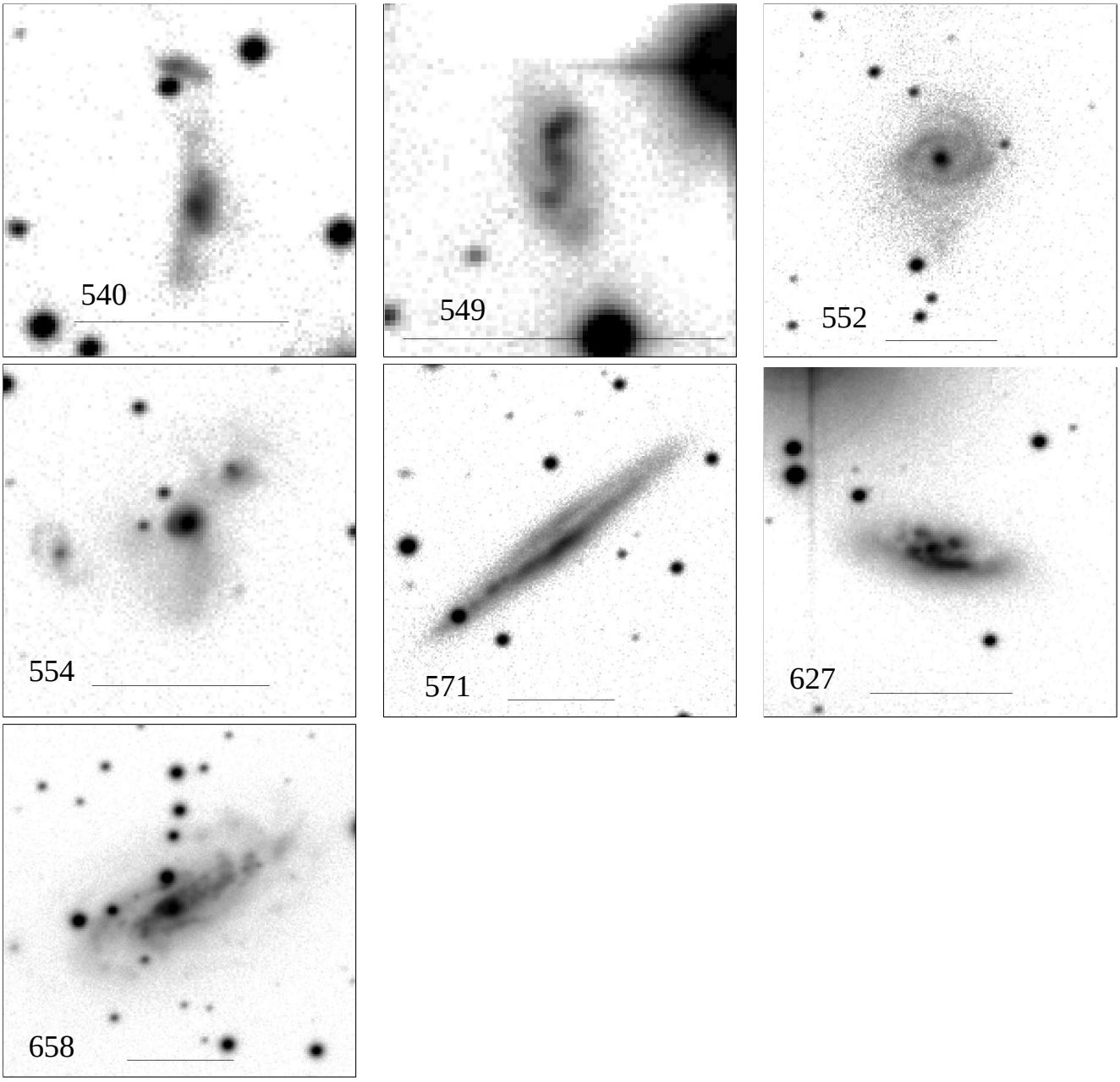

Fig. A.1. (continued)

image and is also indicated in the B band image. One of the most pronounced Hα filaments (pointing towards N) seems to be a coherent structure with a projected length of at least 50 h_{50}^{-1} kpc. It is not clear whether the many peculiarities of this galaxy are related either to a recent merger, or to the cooling flow, or to the interaction of the strong radio source (3C84) with the cluster gas. The HST WFPC2 image shows a highly structered inner region with indications of faint pieces of spiral arms and patchy absorption.

342 A symmetrical, nearly face-on disk galaxy showing a pronounced bar and weak outer ring structure. The bar and the nucleus are bright in the B band and in the Hα image. There are no outer spiral arms. The galaxy was host of SN 1958 E, which was located, according to its catalogued coordinates (Barbon et al. 1989), near the ring.

383/384 This is one of the most spectacular interacting/merging systems in our sample with two spirals embedded in a very extended (about $1'$ in E-W) common halo. The projected core distance of the nuclei is $10''$, the separation in velocity space amounts to 133 km s^{-1}. The central region of the upper galaxy (no. 383) is very bright.

538 A barred spiral with inner ring showing several bright knots in the arms (superposed by a foreground star about $8''$ W).

540 A distant system interacting with a spiral (?) at core distance of about $20''$. The northern galaxy exhibits a tidal tail towards the companion. The southern galaxy appears more disturbed and resembles the well-known Antennae galaxy (Arp 244).

549 The interpretation is hampered by two bright foreground stars and by the small size of the system. The brightness distribution is clearly asymmetric. On lower resolution images, the galaxy shows a head-tail structure. According to its asymmetry, we classified this system as "obviously disturbed". At 1" seeing (Fig. A.1), the galaxy appears at first glance as a two-armed spiral, but the brightness distribution is clearly non-symmetric with the brightness centre northward of the geometric centre. The galaxy 549 is probably the most uncertain member of subgroup **A**. A high resolution VLA contour map at 1.425 GHz is shown by Condon et al. (1996).

552 A spiral with two weak inner arms (perhaps an inner ring?). The spiral structure is embedded in a faint outer envelope of irregular shape, which can be traced up to $> 1.5\, r_{25}$. A region of enhanced surface brightness about $20''$ S of the nucleus may be a faint companion of low surface brightness.

554 A compact group of, at least, three galaxies in a common halo within a radius of about $30''$. At least two galaxies are interacting giving rise to a complex structure (perhaps a multiple merger) and a very pronounced emission-line nucleus.

571 A big late-type spiral with pronounced absorption seen nearly edge-on. The large-scale structure appears quite regular and planar. The projected distance to the SBR galaxy IC 320 (576) is only $3'$, but the separation in velocity space is more than $3\,000\,\mathrm{km\,s^{-1}}$.

627 The structure analysis of this galaxy is hampered by a nearby very bright foreground star. The inner part of this galaxy is very irregular, with bright knots and peculiar dust absorption. The galaxy is identified with the radio source B3 0325+400 from the Bologna 408 MHz survey (Ficarra et al. 1985).

658 Apparently a spiral with bar. Both the B band image and the Hα image reveal a complex, clearly distorted structure. The galaxy is identified with the radio source B3 0326+417 from the Bologna 408 MHz survey (Ficarra et al. 1985) and with a starburst galaxy from the Pico dos Dias Survey (Coziol et al. 1998).

References

Abadi M.G., Morre B., Bower R.G., 1999, MNRAS 308, 947
Abraham R.G., Smecker-Hane T.A., Hutchings J.B., et al., 1996, ApJ 471, 694
Balogh M.L., Morris S.L., Yee H.K.C., Carlberg R.G., Ellington E., 1997, ApJ 488, L75
Balogh M.L., Morris S.L., Yee H.K.C., Carlberg R.G., Ellington E., 1999, ApJ 527, 54
Barbon R., Cappellaro E., Turatto M., 1989, A&AS 81, 421
Barnes J.E., Hernquist L., 1996, ApJ 471, 115
Barton E.J., Geller M.J., Kenyon S.J., 2000, ApJ 530, 660
Bekki K., 1998, ApJ 499, 635
Boisson C., Joly M., Moultaka J., Pelat D., Serote Roos M., 2000, A&A 357, 850
Bothun G.D., Schommer R.A., 1982, AJ 87, 1368
Bothun G.D., Dressler A., 1986, ApJ 301, 57
Brunzendorf J., Meusinger H., 1999, A&AS 139, 141 (paper 1)
Bushouse H.A., 1986, AJ 91, 255
Bushouse H.A., Lamb S.A., Werner M.W., 1988, ApJ 335, 74
Butcher H., Oemler A., 1994, ApJ 285, 426
Calcáneo-Roldán C., Moore B., Bland-Hawthorn J., Malin D., Sadler E.M., 2000, MNRAS 314, 324
Clements D.L., Sutherland W.J., Saunders W., et al., 1996a, MNRAS 279, 459
Clements D.L., Sutherland W.J., McMahon R.G., Saunders W., 1996b, MNRAS 279, 477
Condon J.J., Anderson M.L., Helou G., 1991, ApJ 376, 95
Condon J.J., Helou G., Sanders D.B., Soifer B.T., 1996, ApJS 103, 81
Couch W.J., Barger A.J., Smail I., Ellis R.S., Sharples R.M., 1998, ApJ 497, 188
Coziol R., Torres C.A.O., Quast G.R., Contini T., Davoust E., 1998, ApJS 119, 239
Crawford T., Marr J., Partridge B., Strauss M.A., 1996, ApJ 460, 225
Cunow B., 1992, A&A 268, 491
Dressler A., Gunn J.E., 1983, ApJ 270, 7
Dressler A., Oemler A., Butcher H.R., Gunn J.E., 1994, ApJ 430, 107
Evrard A.E., 1991, MNRAS 248, 8
Ficarra A., Grueff G., Tomassetti G., 1985, A&AS 59, 225
Froebrich D., Meusinger H., 2000, A&AS, in press
Fujita Y., 1998, ApJ 509, 587
Fujita Y., Nagashima M., 1999, ApJ 516, 619
Fullmer L., Lonsdale C., 1989, Catalogued Galaxies and Quasars Observed in the IRAS Survey. Version 2, Jet Propulsion Laboratory, Pasadena
Ghigna S., Moore B., Governato F., et al., 1998, MNRAS 300, 146
Gisler G.R., Miley G.K., 1979, A&A 76, 109
Gunn J.E., Gott R.R., 1972, 176, 1
Hashimoto Y., Oemler A., 2000, ApJ 530, 652
Henriksen M.J., Byrd G., 1996, ApJ 459, 82
Hewitt A., Burbidge G., 1991, ApJS 75, 297
Hibbard J.E., van Gorkom J.H., 1996, AJ 111, 665
Joseph R.D., Meikle W.P.S., Robertson N.A., Wright G.S., 1984, MNRAS 209, 111
Joseph R.D., Wright G.S., 1985, MNRAS 214, 87
Kennicutt R.C., 1998, ARA&A 36, 189
Kent S.M., Sargent W.L.W., 1983, AJ 88, 697
Kim D.-C., Sanders D.B., 1998, ApJS 119, 41
Klaas U., Elsässer H., 1993, A&AS 99, 71
Larson R.B., Tinsley B.M., 1978, ApJ 219, 46
Leech K.J., Lawrence A., Rowan-Robinson M., et al., 1990, In: Wielen R. (ed.) Dynamics and Interactions of Galaxies. Springer, Heidelberg, p. 153
Leggett S.K., Clowes R.G., Kalafi M., et al., 1987, MNRAS 227, 563
Leitherer C., 1998, In: Gilmore G., Howell D. (eds.) The Stellar Initial Mass Function. ASP Conf. Ser. 142, p. 61
Lutz D., 1992, A&A 259, 462
Meusinger H., Brunzendorf J., Froebrich D., Krieg R., 1999, In: Kroll P., la Douz C., Bräuer H.-J. (eds.) Treasure Hunting in Astronomical Plate Archives. H. Deutsch, Frankfurt, p. 223
Mihos J.C., Hernquist L., 1996, ApJ 464, 641
Moore B., Lake G., Katz N., 1998, ApJ 495, 139
Murphy T.W., Armus L., Matthews K., et al., 1996, AJ 111, 1025
Noguchi M., Ishibashi S., 1986, MNRAS 219, 657
Noguchi M., 1990, In: Thronson H.A., Shull J.M. (eds.) The Interstellar Medium in Galaxies. Kluwer, Dordrecht, p. 323

Quilis V., Moore B., Bower R., 2000, Sci 288, 1617
Rakos K.D., Odell A.P., Schombert J.M., 1997, ApJ 490,, 194
Rhee G., Burns J.O., Kowalski M.P., 1994, AJ 108, 1137
Rigopoulou D., Spoon H.W.W., Genzel R., et al., 1999, AJ 118, 2625
Rowan-Robinson M., Crawford J., 1989, MNRAS 238, 253
Sanders D.B., Scoville N.Z., Young J.S., et al., 1986, ApJ 305, L45
Sanders D.B., Egami E., Lipari S., Mirabel I.F., Soifer B.T., 1995, AJ 110,, 1993
Sanders D.B., Mirabel I.F., 1996, ARA&A 34, 749
Schweizer F., 1976, ApJS 31, 313
Siegel S., Castellan N.J., 1988, Nonparametric Statistics for the Behavioral Sciences. McGraw-Hill, Inc., New York
Smith D.A., Herter T., Haynes M.P., et al., 1996, ApJS 104, 217
Soifer B.T., Sanders D.B., Neugebauer G., et al., 1986, ApJ L303, 29
Soifer B.T., Houck J.R., Neugebauer G., 1987, ARA&A 25, 187
Soifer B.T., Neugebauer G., 1991, AJ 101, 354
Solomon P.M., Sage L.J., 1988, ApJ 334, 613
Stein W.A., 1988, AJ 96, 1861
Theys J.C., Spiegel E.A., 1977, ApJ 212, 616
Thuan T.X., Sauvage M., 1992, A&AS 92, 749
Toomre A., Toomre J., 1972, ApJ 178, 623
Whitmore B.C., Lucas R.A., McElroy D.M., et al., 1990, AJ 100, 1489
Wise M.W., O'Connell R.W., Bregman J.N., Roberts M.S., 1993, ApJ 405, 94
Young J.S., Allen L., Kenney J.D.P., Lesser A., Rownds B., 1996, ApJ 112, 1903
Yuan Q.R., Zhu Z.H., He X.T., 1996, A&AS 115, 267